Optical intersubband transitions in conduction-band quantum wells

Rui Q. Yang
Space Vacuum Epitaxy Center, University of Houston, Houston, Texas 77204-5507
and CYC Technologies, Toronto, Canada
(Received 21 September 1994; revised manuscript received 10 July 1995)

In this work, theoretical formulation for optical intersubband transitions has been developed within the framework of a simple one-band model by including the spatial variation of effective mass in quantum-well heterostructures. It has been shown how the in-plane polarized optical inter-conduction-subband transitions could be made large in direct-band-gap semiconductor quantum wells. However, calculations have confirmed that the normal-to-plane polarized optical intersubband transition is still dominant. The dependence of optical intersubband transitions on quantum-well structure geometry and parameters has been investigated, which provides insights to the underlying physics, and suggests a way how experiments could be carried out to examine these physical phenomena related to optical intersubband transitions.

I. INTRODUCTION

Rapid progress has been made in both the physics of intersubband transitions in quantum-well (QW) structures and device applications such as infrared photodetectors.[1] However, the present understanding and the related device development have been limited by the common belief that the in-plane polarized optical intersubband transition in a conduction-band QW is forbidden. This has resulted in the nearly universal adoption of the Brewster angle, the 45° bevel angle or the diffraction grating for optical coupling.[1] This brings technical complications to the device fabrication and system implementation. In order to avoid such complications, normal-incidence (i.e., incident light with the in-plane polarization) p-type QW infrared photodetectors based on inter-valence-subband transitions have been sought and demonstrated,[2–5] where the band mixing between light and heavy holes plays the critical role. Also, normal-incidence QW photodetectors based on indirect-band-gap semiconductors with anisotropic effective-mass tensors have been suggested and demonstrated.[6–9] However, complications in design and controllability would result from involving various valence bands with different dispersions or tilted ellipsoidal band structures. Furthermore, the smaller electron effective mass and the higher mobility typical of the conduction band in the Γ valley of a direct-band-gap semiconductor are highly desirable to the detector's sensitivity and speed. Thus normal-incidence photodetectors based on an n-type conduction-band QW system in direct-band-gap semiconductors are more preferable. Recently, a few theoretical efforts have been devoted to exploring some possible mechanisms[10–16] for the in-plane polarized optical inter-conduction-subband transition in a direct-band-gap semiconductor system, which include the nonparabolicity of a bulk semiconductor band structure with sophisticated multiband schemes, the symmetry breaking of a real QW structure, and the strain effect with the group-theoretical approach. Also, experimental evidence of electron intersubband normal-incidence absorption was reported for direct-band-gap semiconductor QW structures,[17–19] but the mechanisms responsible for the transitions are not clear yet. Whether the normal-incidence absorption can be realized with n-type direct band-gap semiconductor QW structures is still an open question. In this work, within the framework of a simple one-band model, we shall examine the polarization dependence of optical inter-conduction-subband transitions in direct-band-gap semiconductor QW structures by considering the spatial variation of effective mass on an equal footing. Also, we shall investigate how optical intersubband transitions are related to the QW structure parameters, which may provide an accessible way for experimental testing.

II. ONE-BAND MODEL

In a simple one-band scheme, the wave function for a given QW structure may be written as

$$\Psi(\mathbf{r})=\frac{1}{\sqrt{S}}\exp(i\mathbf{k}_{\parallel}\rho)\varphi(z)\ , \tag{1}$$

where S is the sample area, $\mathbf{k}_{\parallel}=(k_x,k_y)$ the two-dimensional (2D) in-plane wave vector, $\rho=(x,y)$ the 2D coordinate space vector, and $\mathbf{r}=(\rho,z)$. $\varphi(z)$ is a slowly varying envelope function in the growth direction, z, and is determined by BenDaniel and Duke's effective-mass equation,[20] i.e.,

$$\left[\mathbf{P}\frac{1}{2m^*(z)}\mathbf{P}+V(z)\right]\exp(i\mathbf{k}_{\parallel}\rho)\varphi(z)=E\exp(i\mathbf{k}_{\parallel}\rho)\varphi(z)\ . \tag{2}$$

$\mathbf{P}=-i\hbar\nabla$ is the momentum operator, $V(z)$ refers to the potential energy in a QW structure, E is the electron energy, and $m^*(z)$ is the spatially dependent effective mass. With boundary conditions that require the continuity of the envelope function $\varphi(z)$ and its derivative over the effective mass, one can solve Eq. (2) in a standard procedure, obtaining the energy eigenvalue E_n and eigen-

function $\varphi_n(z)$ for the nth subband. For a QW structure which is symmetric under the reflection $z \rightarrow -z$, one can find that eigenfunctions $\varphi_n(z)$ have even parity for all odd levels ($n=1,3,\ldots$), and odd parity for all even levels ($n=2,4,\ldots$).

The effective-mass equation (2) has been widely used for calculating the energy levels and envelope functions of electronic states in semiconductor QW heterostructures. A further justification for its use was recently given by Burt with a direct derivation of the effective-mass equation for QW structures.[21] In the presence of a photon field, within an effective-mass framework,[22,23] replacing $\mathbf{P}$ by $\mathbf{P}+(e/c)\mathbf{A}$ in Eq. (2), an effective electron-photon interaction Hamiltonian can be written as

$$H_{\text{int}}=\frac{e\,\mathbf{A}}{2c}\cdot\left[\frac{1}{m^*}\mathbf{P}+\mathbf{P}\frac{1}{m^*}\right], \tag{3}$$

where $\mathbf{A}$, e, and c denote the vector potential, the electron charge, and the speed of the light, respectively. Equation (3), which takes the spatial variation of an effective mass into account, may not be readily accepted by some readers. In fact, using Burt's method[21] or adopting a multiband model under the spatially varying effective-mass approximation,[15] one can derive Eq. (3) at a fundamental level where the electron-photon interaction is related to the free-electron mass m_0, which is shown in the Appendix. In the framework of the multiband model, the intersubband transition is determined mainly by the mixing of the conduction- and valence-band states due to the band coupling, which is position dependent in QW heterostructures. Such a band coupling is implicitly included in the one-band scheme, and essentially represented by the effective mass. We note that a sophisticated multiband model is more desirable for accurate calculations. However, in this work we will confine the discussion to the one-band model, which is much simpler and more illuminating than a multiband approach.

According to Fermi's golden rule, the optical transition rate between the nth subband and n'th subband is

$$\begin{aligned}R&=\frac{2\pi}{\hbar}|\langle\Psi_n|H_{\text{int}}|\Psi_{n'}\rangle|^2\delta(E_{n'}-E_n-\hbar\omega)\\&=\frac{2\pi e^2}{\hbar c^2 S^2}\left|\frac{\mathbf{A}}{2}\cdot\langle e^{i\mathbf{k}_\parallel\rho}\varphi_n|\frac{1}{m^*}\mathbf{P}\right.\\&\quad\left.+\mathbf{P}\frac{1}{m^*}|e^{i\mathbf{k}_\parallel\rho}\varphi_{n'}\rangle\right|^2\delta(E_{n'}-E_n-\hbar\omega),\end{aligned} \tag{4}$$

where ω is the photon frequency, and the spatial variation of the photon field has been neglected because the wavelength of light is normally much larger than the QW scale. Here the δ function has units of energy^{-1} and indicates the energy conservation, which implicitly assumes that R refers to a single transition process within a continuum of states owing to the continuous in-plane wave vector $\mathbf{k}_\parallel$. To evaluate the total transition rate, one has to integrate R in $\mathbf{k}_\parallel$ space using the density of states, and the singularity introduced by the δ function would disappear after the integration. Considering the presence of scattering in practical devices, the δ function can be replaced by the line broadening function $L(E_{n'}-E_n-\hbar\omega)$, which is often taken to be the Lorentzian line-shape function.[24]

Assuming that the polarization is solely in the x direction, one can simplify Eq. (4) to

$$R_x=\frac{hA^2e^2}{c^2}k_x^2\left|\langle\varphi_n|\frac{1}{m^*(z)}|\varphi_{n'}\rangle\right|^2\delta(E_{n'}-E_n-\hbar\omega), \tag{5}$$

which is proportional to the in-plane wave-vector square. Consequently, the optical-absorption quantum efficiency[24] $\eta_x(\hbar\omega)$ can be written as

$$\begin{aligned}\eta_x(\hbar\omega)=\frac{2\pi\hbar^2e^2}{n_i c\omega}\int k_\parallel^3\left|\langle\varphi_n|\frac{1}{m^*(z)}|\varphi_{n'}\rangle\right|^2\\\times L(E_{n'}-E_n-\hbar\omega)(f_{n'}-f_n)dk_\parallel,\end{aligned} \tag{6}$$

where n_i is the refractive index, f_n is the Fermi-Dirac distribution function, and the line broadening function $L(E_{n'}-E_n-\hbar\omega)$ reduces to a δ function in the absence of scattering.

If the spatial variation of the effective mass in QW structures is ignored, the overlap integral $\langle\varphi_n|(1/m^*)|\varphi_{n'}\rangle$ in Eq. (5) vanishes due to the orthogonality of eigenfunctions, and the in-plane polarized optical intersubband transition is forbidden. In most previous studies, this conclusion was reached by first calculating the dipole matrix element[25] or momentum matrix element[22] without considering the spatial dependencies. However, the inverse effective mass could vary substantially in nanometer scale, which is comparable to the electron de Broglie wavelength, and thus the inverse effective-mass term, which originates from the effective electron-photon interaction Hamiltonian $\mathbf{H}_{\text{int}}$ as shown in Eq. (3), cannot be taken out from the overlap integral in Eq. (5). Applying Eq. (2) to the two eigenstates φ_n and $\varphi_{n'}$, with eigenvalues E_n and $E_{n'}$, respectively, after some algebra one can find

$$\begin{aligned}\langle\varphi_n|\frac{1}{m^*}|\varphi_{n'}\rangle=\frac{\hbar^2}{2(E_{n'}-E_n)}\int\left[\frac{\varphi_n^*}{m^*}\frac{d\varphi_{n'}}{dz}-\frac{\varphi_{n'}}{m^*}\frac{d\varphi_n^*}{dz}\right]\\\times d\left[\frac{1}{m^*}\right].\end{aligned} \tag{7}$$

which is not zero with the spatial variation of the effective mass, making the in-plane polarized optical intersubband transition possible.

Commonly, the oscillator strength[26] $F_{x(z)}(\hbar\omega)$ is used as a measure of optical transitions, in terms of which the optical-absorption quantum efficiency $\eta_{x(z)}(\hbar\omega)$ can be expressed as

$$\begin{aligned}\eta_{x(z)}(\hbar\omega)=\frac{2\pi^2\hbar e^2}{m_0 n_i c}\sum_{\mathbf{k}_\parallel}\frac{1}{S}F_{x(z)}(\hbar\omega)\\\times L(E_{n'}-E_n-\hbar\omega)(f_{n'}-f_n),\end{aligned} \tag{8}$$

where m_0 is the free-electron mass, and subscript x (or z) denotes polarization in the x (or z) direction. Here the oscillator strength is defined as

$$F_{x(z)}(\hbar\omega)=\frac{2}{m_0\hbar\omega}2|M_{x(z)}|^2 , \tag{9}$$

where the extra factor 2 in front of $|M_{x(z)}|^2$ accounts for the twofold spin degeneracy,[15] and $M_{x(z)}$ is the momentum matrix element. For the in-plane polarization, using Eqs. (6), (8), and (9), one can express M_x as[23]

$$M_x=\hbar k_x\langle\varphi_n|(m_0/m^*)|\varphi_{n'}\rangle . \tag{10}$$

Similarly, for the z polarization (normal to plane), the momentum matrix element M_z can be obtained:

$$\begin{aligned}M_z&=\langle\varphi_n|\frac{m_0}{2m^*(z)}P_z+P_z\frac{m_0}{2m^*(z)}|\varphi_{n'}\rangle\\&=M_{zs}+M_{za} ,\end{aligned} \tag{11a}$$

where $P_z=-i\hbar\partial/\partial z$ is the momentum operator in the z direction,

$$M_{zs}=\langle\varphi_n|\frac{m_0}{m^*(z)}P_z|\varphi_{n'}\rangle \tag{11b}$$

is a standard momentum matrix element for the z-polarized optical intersubband transition, and

$$M_{za}=\left\langle\varphi_n|\varphi_{n'}P_z\frac{m_0}{2m^*(z)}\right\rangle \tag{11c}$$

is an additional momentum matrix component M_{za} arising merely from the spatial variation of the effective mass. Usually, an internal angle θ of incidence is associated with the z-polarized optical intersubband transition,[24] and then the optical-absorption quantum efficiency $\eta_z(\hbar\omega)$ is given by

$$\begin{aligned}\eta_z(\hbar\omega)=\frac{2\pi e^2}{n_i c\omega}\frac{\sin^2\theta}{\cos\theta}\int k_\parallel\Bigg|\langle\varphi_n|\frac{1}{m^*(z)}P_z\\+P_z\frac{1}{m^*(z)}|\varphi_{n'}\rangle\Bigg|^2\\\times L(E_{n'}-E_n-\hbar\omega)(f_{n'}-f_n)dk_\parallel .\end{aligned} \tag{12}$$

In the above, a theoretical formulation of optical intersubband transitions has been developed within the framework of a simple one-band model by including the spatial variation of effective mass in QW heterostructures. One can find that considering the spatial variation of effective mass would make a correction to the result obtained from the widely used conventional one-band theory.[22,24] Such a correction may not be significant in the case of the z-polarized optical intersubband transitions in a QW structure. However, the one-band theory which considers the spatially varying effective mass indicates that the commonly believed forbidden in-plane polarized optical inter-conduction-subband transition can occur in direct-band-gap semiconductor QW heterostructures. The significance is that the normal-incidence infrared photodetector could be made based on n-type QW structures. However, at this stage, it is not yet clear whether the in-plane polarized optical intersubband transition due to the mechanism of spatially varying effective mass is detectable, and how it depends on the structure parameters compared with the z-polarized optical intersubband transition, which is important for an experimental test and practical device applications. In Sec. III, the in-plane and z-polarized optical interconduction-subband transitions in QW structures with different configurations will be calculated and discussed, in an attempt to find distinct characteristics for different polarizations and achieve a thorough understanding to the underlying physics.

III. CALCULATIONS AND DISCUSSIONS

We will consider symmetric and asymmetric QW structures in Secs. III A and III B, respectively.

A. Symmetric QW structures

For a symmetric QW structure, the eigenfunctions $\varphi_n(z)$ have definite even or odd parity. Thus the selection rule for the in-plane polarized optical intersubband transition is that the energy-level index difference must be an even integer ($\Delta n=n'-n=2,4,\ldots$) because φ_n and $\varphi_{n'}$ must have the same parity for a nonzero overlap integral [see Eq. (5)], which contrasts sharply with the selection rule for the z-polarized optical intersubband transition ($\Delta n=n'-n=1,3,\ldots$).

Figure 1 shows the calculated results of the ratio of

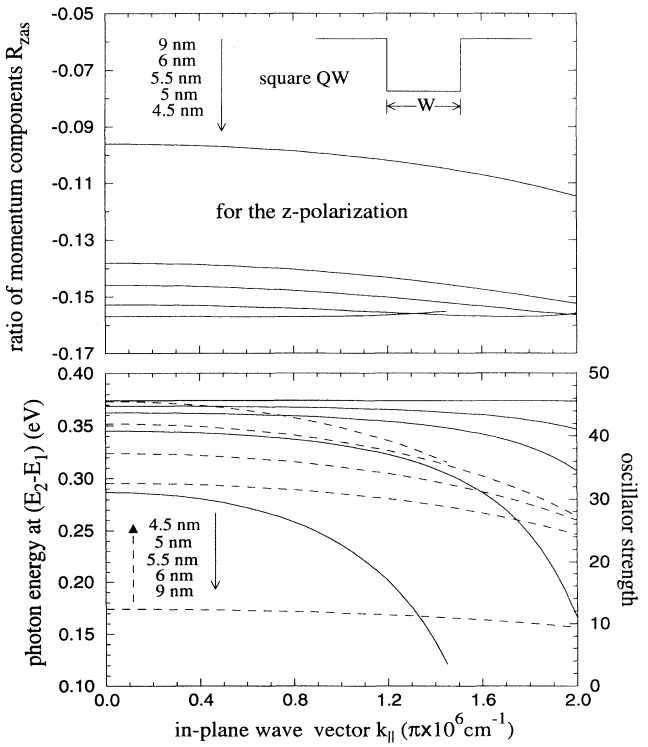

FIG. 1. Calculated results of the ratio of momentum components, $R_{zas}=M_{za}/M_{zs}$, and the z-polarized optical transition oscillator strength (solid) at the photon energy (dashed) $\hbar\omega(=E_2-E_1)$ for $In_{0.53}Ga_{0.47}As/In_{0.52}Al_{0.48}As$ square QW's with different well widths listed in the figure.

momentum components, $R_{zas}=M_{za}/M_{zs}$, and the oscillator strength F_2 at the photon energy $\hbar\omega(=E_2-E_1)$ which equals the energy separation between the first and second energy levels, for $In_xGa_{1-x}As/Al_xGa_{1-x}As$ square QW's with z-polarized light. Because of the effective-mass difference between the well and barrier materials, the effective potential energy in QW structures changes as the in-plane wave vector $k_\parallel$ varies,[27,28] which leads to a nonparabolic dispersion relation $(E-k_\parallel)$ for each subband in a QW structure, though a bulk parabolic dispersion relation (energy-independent effective mass) is assumed for each material. Consequently, the energy separation between subbands is not constant when the in-plane wave vector $k_\parallel$ changes. Also, the ratio R_{zas} and oscillator strength vary with the in-plane wave vector $k_\parallel$ for the same reason. From Fig. 1, one finds that the ratio R_{zas} is negative. This means that M_{za} and M_{zs} make opposite contributions to the momentum matrix element M_z. When the well width is small, the amplitude of M_{za} is relatively larger, but is still insignificant to the z-polarized optical intersubband transition. Thus M_{za} can be neglected without a significant change of results. When the well is wide, electrons are confined in the well, and the oscillator strength F_z is approximately $2m_0/m^*$, being independent of the well width, which reduces to the result obtained from an infinite deep potential-well model.[25] When the well width is narrow, the wave function φ_2 of the second electronic state substantially extends to the barrier region, reducing the confinement in the well region as shown by the moderate increase of the energy separation between subbands. Thus the oscillator strength F_z becomes smaller. This is because the momentum matrix element for a transition between two states is critically determined by the overlap of their wave functions, which decreases when one of the wave functions becomes more extended in real space with reduced amplitude. This also agrees with the previous finding that the z-polarized optical intersubband transition decreases as the well width becomes smaller.[24] The variation of the oscillator strength with the in-plane wave vector $k_\parallel$, as shown in Fig. 1, which was not considered in previous studies, also demonstrates the features of optical intersubband transitions related to the confinement of electrons. Since the effective mass is larger in the barrier layer than in the well layer, the electron confinement within the well is reduced and the second level is pushed toward the top of the effective potential well with increasing $k_\parallel$, leading to a significant decrease of the oscillator strength. When the in-plane wave vector $k_\parallel$ is further increased or the well width is reduced such that the second energy level is pushed above the barrier into the continuous spectrum and the transition becomes from a bound state to a quasibound state, the oscillator strength is well below the one for transition between bound states. A cutoff point in Fig. 1 indicates the turning from the bound state to the quasibound state with the increase of $k_\parallel$.

Figure 2 shows the calculated results of the overlap integral, $\langle\varphi_1|(m_0/m^*)|\varphi_3\rangle$, and the oscillator strength F_x at the photon energy $\hbar\omega$ $(=E_3-E_1)$, which equals the energy separation between the first and third energy levels, for $In_xGa_{1-x}As/Al_xGa_{1-x}As$ square QW's with in-plane polarized light. From Fig. 2, one can see that the overlap integral and the oscillator strength F_x change nonmonotonically with the well width and the in-plane wave vector $k_\parallel$. To understand such features, we come to examine the spatial characteristics of wave functions $\varphi_n(z)$.

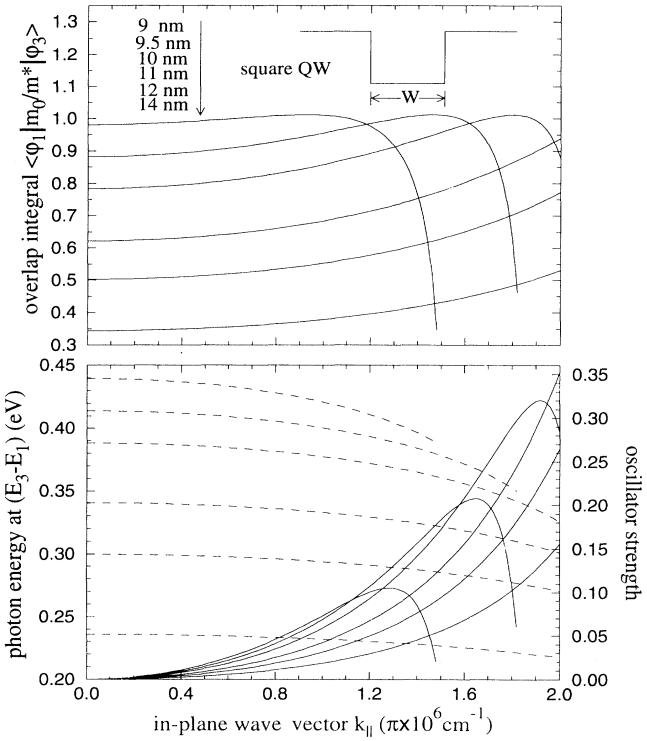

FIG. 2. Calculated results of the overlap integral, and the in-plane polarized optical transition oscillator strength (solid) at the photon energy (dashed) $\hbar\omega(=E_3-E_1)$ for $In_{0.53}Ga_{0.47}As/In_{0.52}Al_{0.48}As$ square QW's with different well widths listed in the figure.

According to the oscillation theorem[29] that the eigenfunction $\varphi_n(z)$ corresponding to the nth energy eigenvalue E_n vanishes $(n-1)$ times, φ_3 has two nodes at z_0 and $-z_0$ as shown in Fig. 3. Since the wave function φ_3 is positive in region I (from $-z_0$ to z_0) and becomes negative in region II (from $-\infty$ to $-z_0$ and z_0 to ∞), the integral $\int_I\varphi_1(m_0/m^*)\varphi_3dz$ in region I and the integral $\int_{II}\varphi_1(m_0/m^*)\varphi_3dz$ in region II make opposite contributions to the overlap integral $\langle\varphi_1|(m_0/m^*)|\varphi_3\rangle$. The inverse effective-mass term in the overlap integral acts like a local weight of the wave function, which gives a measure of how electrons in different positions contribute to the optical transition. If the effective mass m^* is a constant over the whole space, electrons in different positions contribute the same weight to the optical transition, and the overlap integrals in regions I and II cancel out due to the orthogonality, leading to a forbidden transition and making the weight of the wave function meaningless. However, the effective mass in QW heterostructures varies in real space, and thus the weights for regions I

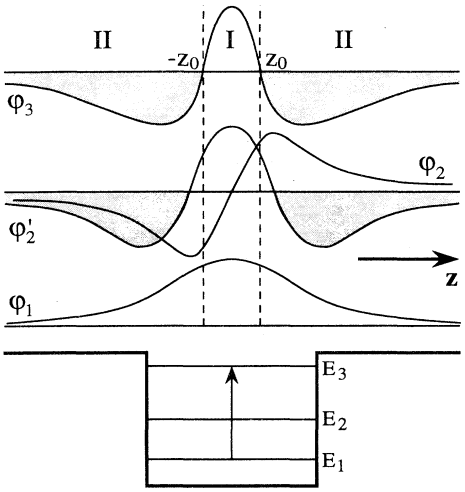

FIG. 3. Schematic illustration of eigenfunctions φ_1, φ_3, φ_2 and its derivative φ_2' (upper part), and the square QW (lower part).

and II can differ substantially, providing a way to manipulate the in-plane polarized optical intersubband transition. We note that the above discussion can also apply to the z-polarized optical intersubband transition, since $\varphi_2'(=d\varphi_2/dz$, derivative) in the momentum matrix element $M_z=i\hbar[\langle\varphi_1|(m_0/m^*)|\varphi_2'\rangle+\int\varphi_1\varphi_2 d(m_0/2m^*)]$ (the first term is dominant) has a spatial feature similar to φ_3, but with two nodes closer to the interfaces as shown in Fig. 3, leading to a nonzero overlap integral $\langle\varphi_1|(m_0/m^*)|\varphi_2'\rangle$.

For square QW's with a finite effective-mass difference in the well and barrier layers, calculated results in Fig. 2 show that the overlap integral $\langle\varphi_1|(m_0/m^*)|\varphi_3\rangle$ and the in-plane polarized optical intersubband transition increase as the well width decreases when the third energy level E_3 is well below the top of the well. This is because the nodes of wave function φ_3 grow closer to the interfaces, making the weight difference between regions I and II larger. On the other hand, when the well width is reduced or the in-plane wave vector $k_{\parallel}$ is larger such that the third energy level is pushed toward the top of the effective potential well, wave function φ_3 would extend to the barrier region, reducing the overlap with wave function φ_1. This will lead to a decrease of the overlap integral $\langle\varphi_1|(m_0/m^*)|\varphi_3\rangle$ and the oscillator strength F_x, which becomes dominant when the third energy level is near or above the top of the effective potential well. Combining the two competing factors discussed above, one can understand the nonmonotonic dependence of the in-plane polarized optical intersubband transition on the well width and the in-plane wave vector. Such a nonmonotonic dependence of the in-plane polarized optical intersubband transition on the well width of the square QW structures is distinct from that of the z-polarized optical intersubband transition, suggesting a way for the experimental study to verify this optical transition mechanism.

Since the nodes of wave function φ_3 for a bound state are always located in the well, there are electrons with smaller effective masses in both regions I and II, which limits the weight difference and leads to small in-plane polarized optical intersubband transitions in the square QW's. When the well width is reduced such that the third energy level is pushed above the barrier into the continuous spectrum and becomes a quasibound state, the nodes can be located on the interfaces, and the maximal difference in weight between regions I and II can be reached. However, the overlap between φ_3 and φ_1 is dramatically reduced due to the significant expansion of wave function φ_3 into the barrier region, as discussed above, which leads to a substantial decrease of the in-plane polarized optical transition between bound state φ_1 and quasibound state φ_3 though the weight difference between regions I and II is larger. Thus the in-plane polarized optical intersubband transition is difficult to observe in conventional square QW's, which agrees with the usual experiments.

From the above analysis, one can conceive that if the nodes of the excited-state wave function can be located on or near the interface of two materials with substantial effective-mass offsets, and, simultaneously, the overlap of wave functions between the two transition states is large in real space, a large in-plane polarized optical intersubband transition can result. This can be done by adjusting the structure geometry and the material compositions through band-gap engineering, with attention paid to the spatial characteristics of wave functions. Two modified QW structures, the symmetric step QW and the coupled double-step QW, as shown in the insets of Figs. 4 and 5, respectively, can have the required features. In these QW structures, inner step QW's make the weights between regions I and II differ substantially, and the outer barrier layers protect the wave function of the third energy state from expansion outside the well region. The calculated results for two modified QW structures are given in Figs. 4 and 5. Though the two structures are not optimized, the overlap integral and the oscillator strength for the in-plane polarized optical intersubband transition are substantially enhanced compared with that in the square QW's.

Figure 6 shows the calculated results of the z-polarized optical transition oscillator strength at the photon energy $\hbar\omega$ $(=E_2-E_1)$ for the $In_xGa_{1-x}As/InP/In_xAl_{1-x}As$ symmetric step QW structures. The oscillator strength and the subband separation decrease as the side layer thickness b increases. This is because the excited-state wave function φ_2 extends farther away from the center well layer, reducing the overlap between φ_2 and φ_1 which is mainly localized in the center well layer. Compared with the square QW, the modified QW structure configuration is more beneficial to the manipulation of optical properties.

As illustrated above, the in-plane polarized optical inter-conduction-subband transition can be made larger by modifying the QW structure configuration through quantum wave-function engineering. However, the in-plane polarized optical inter-conduction-subband transition is generally much smaller than the z-polarized opti-

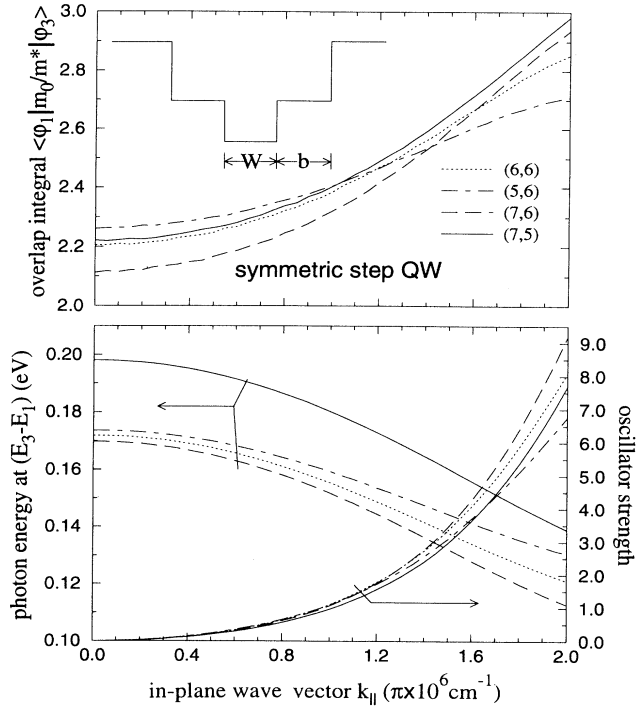

FIG. 4. Calculated results of the overlap integral, the in-plane polarized optical transition oscillator strength at the photon energy $\hbar\omega(=E_3-E_1)$ for $In_{0.53}Ga_{0.47}As/In_{0.77}Ga_{0.23}As_{0.5}P_{0.5}/In_{0.52}Al_{0.48}As$ symmetric step QW's with different structure parameters (W,b) in units of nanometers listed in the figure.

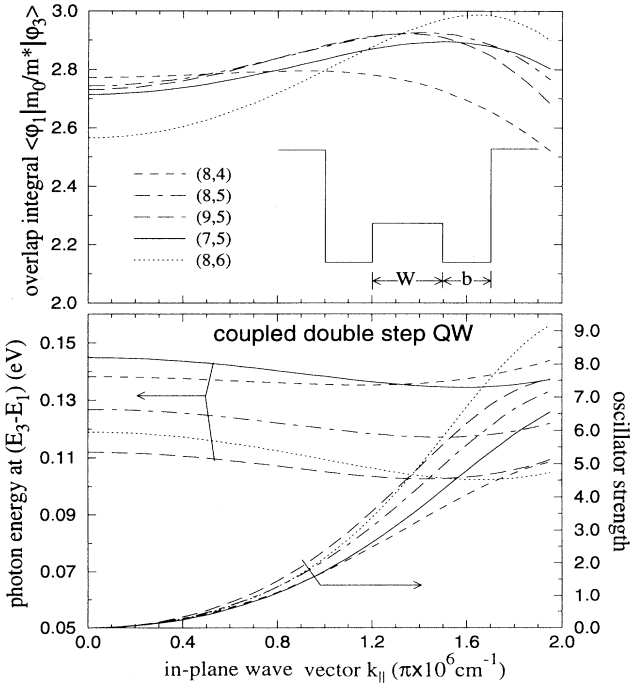

FIG. 5. Calculated results of the overlap integral, the in-plane polarized optical transition oscillator strength at the photon energy $\hbar\omega(=E_3-E_1)$ for $In_{0.53}Ga_{0.47}As/In_{0.77}Ga_{0.23}As_{0.5}P_{0.5}/In_{0.52}Al_{0.48}As$ coupled double-step QW's with different structure parameters (W,b) in units of nanometers listed in the figure.

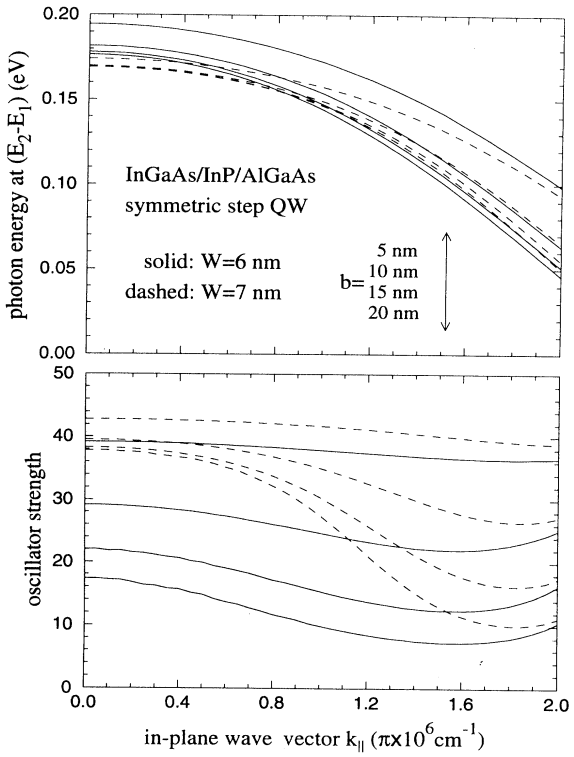

FIG. 6. Calculated results of the z-polarized optical transition oscillator strength at the photon energy $\hbar\omega(=E_2-E_1)$ for $In_{0.53}Ga_{0.47}As/InP/In_{0.52}Al_{0.48}As$ symmetric step QW's with different structure parameters (W,b) listed in the figure.

cal intersubband transition. The equally strong intersubband transitions reported for different polarizations[17,18] cannot be explained by this simple one-band theory, but a similar conclusion could be made by using an eight-band model.[15] Including remote bands with considerations of broken symmetries could produce other possible mechanisms for the in-plane polarized optical inter-conduction-subband transition, which is more complicated and may not be well handled by a perturbation theory, since the result could vary substantially depending on approximations made. Recent numerical calculations by Voon, Willatzen, and Ram-Mohan,[30] based on a more elaborate microscopic model, have confirmed that the influence of remote bands is negligible, and that the in-plane polarized optical inter-conduction-subband transition is much smaller than the z-polarized optical intersubband transition, suggesting the reinterpretation of the above-mentioned experiments.[17,18] Here, using a one-band model which contains the essential physics, we present some features of the optical intersubband transitions related to QW structure configurations and parameters, which can be examined by experiments and may be helpful to the clarification of the confusion in the literature.

Regarding the observed separated absorption peaks for different polarizations reported for $In_xGa_{1-x}As/In_xAl_{1-x}As$ QW's (Ref. 17) and $In_xGa_{1-x}As/GaAs$

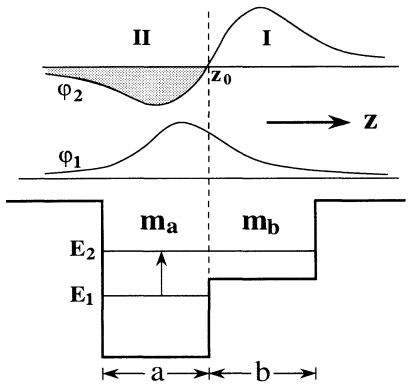

FIG. 7. Schematic illustration of eigenfunctions φ_1 and φ_2 (upper part), and the asymmetric step QW (lower part) which consists of a deep well with the well width a, and a shallow well with the well width b.

QW's,[18] since the absorption peaks have finite widths, and the polarization of a lightwave mode in a waveguide structure can affect the optical field and its interaction with the environment, there is no absolute reason why the absorption peaks for different polarizations should coincide. The observed separated absorption peaks for different polarizations have been interpreted mainly as a result of strain effects,[14] and partially because of the depolarization effect.[18] There may be several mechanisms responsible for such a splitting of different polarized optical-absorption peaks, since strain deformation, interface roughness, many-body effect, and spatial charge transfer and buildup are present in real QW structures. More systematic experimental investigations are needed to provide specific features which can be used to identify different causes.

B. Asymmetric QW structures

For an asymmetric QW structure, the eigenfunctions $\varphi_n(z)$ do not have a definite parity, thus the in-plane polarized optical transition can occur between any pair of subbands. We consider the in-plane polarized optical transition between the first bound state and the second bound state in an asymmetric step QW structure, as shown in Fig. 7. Similarly, the node z_0 of the wave function $\varphi_2(z)$ should be designed to be on or near the interface, as illustrated in Fig. 7, for obtaining a large overlap integral $\langle \varphi_1 | (m_0/m^*) | \varphi_2 \rangle$.

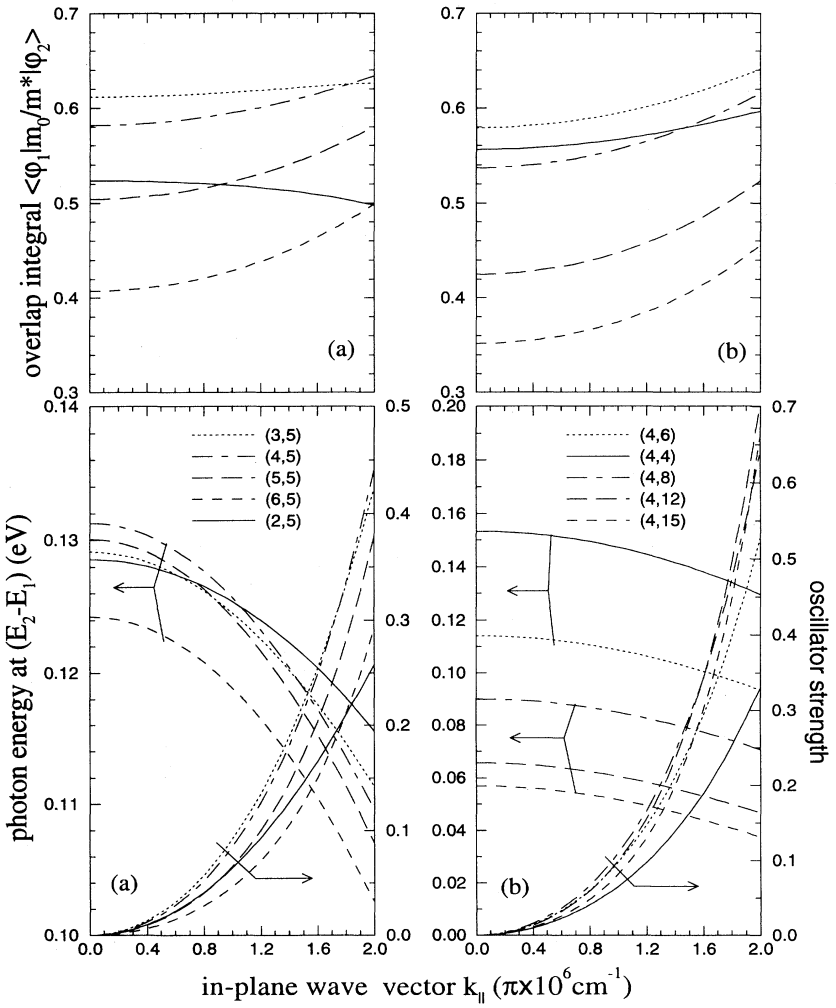

FIG. 8. Calculated results of the overlap integral, and the in-plane polarized optical transition oscillator strength at the photon energy $\hbar\omega(=E_2-E_1)$ for $GaAs/Al_{0.15}Ga_{0.85}As/Al_{0.45}Ga_{0.55}As$ asymmetric step QW's with different structure parameters (a,b) in units of nanometers listed in the figure.

Calculated results of the overlap integral and the oscillator strength at the photon energy $\hbar\omega(=E_2-E_1)$ for $GaAs/Al_{0.15}Ga_{0.85}As/Al_{0.45}Ga_{0.55}As$ asymmetric step QW's are shown in Fig. 8. One can find that as the deep well width a decreases with the fixed shallow well width b, as shown in Fig. 8(a), the overlap integral and the oscillator strength first increase because the node of wave function $\varphi_2(z)$ is pushed from the inside of the deep well toward the interface with the shallow well, and then decrease after the node of wave function $\varphi_2(z)$ is pushed over the interface and into the shallow well when the deep well width becomes small. The energy separation between the first level E_1 and the second level E_2 also changes with the deep well width a, which shows a nontrivial dependence on the in-plane wave vector $k_{\parallel}$, attributed to the variation of electron confinement due to the combined effect of the potential-energy difference and the effective-mass difference. Fixing the deep well width a and changing the shallow well width b as shown in Fig. 8(b), the overlap integral shows a similar variation, but the oscillator strength has a somewhat different dependence because the energy separation changes more drastically, corresponding to different photon wavelength regions.

One can enhance the effective-mass difference between the deep and shallow wells by using a relatively wider band-gap material $Al_{0.2}Ga_{0.8}As$ instead of $Al_{0.15}Ga_{0.85}As$ to increase the overlap integral and the oscillator strength. The calculated results of the overlap integral and the oscillator strength at the photon energy $\hbar\omega(=E_2-E_1)$ for $GaAs/Al_{0.2}Ga_{0.8}As/Al_{0.45}Ga_{0.55}As$ asymmetric step QW's, as shown in Fig. 9, indicate the feasibility of obtaining more desirable optical properties by adjusting the material composition. The recent observation of surface-emitting second-harmonic generation by inter-conduction-subband transitions reported for $GaAs/Al_xGa_{1-x}As$ asymmetric step QW's (Ref. 19) is indicative of the occurrence of in-plane polarized optical intersubband transitions, which was questioned by Berger, Bois, and Rosencher.[31] Since the observed Fourier transform absorption spectrum of the waveguiding sample[19] could come from both TE and TM active intersubband transitions, direct comparison cannot be made with our calculations. Further experiments are expected to clarify this controversial issue.

IV. CONCLUDING REMARKS

In summary, optical inter-conduction-subband transitions in QW structures have been investigated, with an

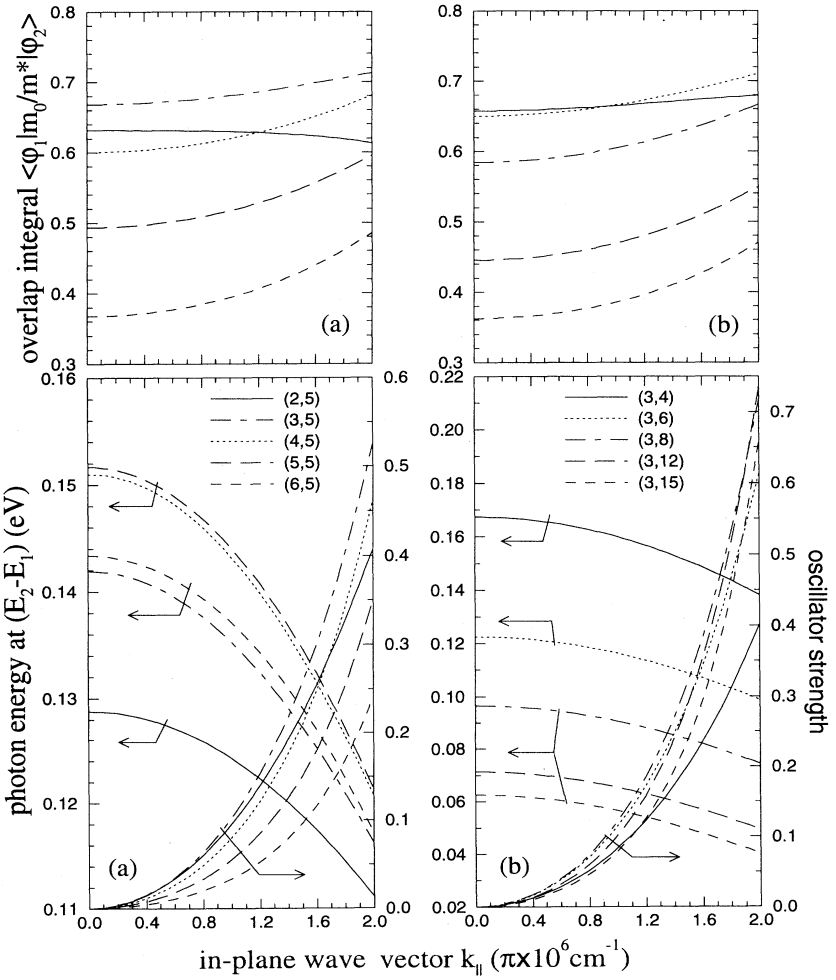

FIG. 9. Calculated results of the overlap integral, the in-plane polarized optical transition oscillator strength at the photon energy $\hbar\omega(=E_2-E_1)$ for $GaAs/Al_{0.2}Ga_{0.8}As/Al_{0.45}Ga_{0.55}As$ asymmetric step QW's with different structure parameters (a,b) in units of nanometers listed in the figure.

emphasis on the polarization dependence and specific features related to the structure configurations and parameters. It has shown that the in-plane polarized optical intersubband transition due to the spatial variation of the effective mass could be made large in a conduction-band QW through quantum wave-function engineering. However, based on our calculations, the in-plane polarized optical intersubband transition is still much smaller than the z-polarized optical intersubband transition. Thus, using the in-plane polarized optical intersubband transition instead of the dominant z-polarized optical intersubband transition may not be beneficial to the photodetection, though a normal-incidence scheme could be realized. On the other hand, the possible in-plane polarized optical intersubband transition opens up opportunities for interesting nonlinear optical properties in QW heterostructures. Since the flexibility provided by band-gap engineering for QW structures, near-resonance intersubband transitions are possible, and the asymmetry of the envelope wave function can be easily manipulated. This can lead to large nonlinear optical coefficients such as the second-order susceptibility $\chi^{(2)}$. Therefore, it is possible to observe surface-emitting second-harmonic generation based on inter-conduction-subband transitions in asymmetric QW structures. The dependence of optical intersubband transitions on QW structure geometry and parameters revealed in this work suggests a way in which experiments could be carried out to examine these physical phenomena related to optical intersubband transitions.

ACKNOWLEDGMENTS

This research was started while the author was at the University of Toronto, where part of the paper was completed, and is partially supported by NASA Contract No. NAGW-977 and the Texas Center for Superconductivity. The author is grateful to Claudio Aversa, H. C. Liu, and M. Sweeny for useful discussions, and Keith Lee, Stephen O'Leary, and S. Zukotynski for their helpful comments and critical reading of an early version of this manuscript.

APPENDIX

In the framework of a multiband model, the eigenfunction $\Psi_n(\mathbf{r})$ for the nth subband with eigenenergy E_n can be written as

$$\Psi_n(\mathbf{r})=\sum_j F_{nj}(\mathbf{r})U_j(\mathbf{r}) , \tag{A1}$$

where $F_{nj}(\mathbf{r})$ is the envelope function, and $U_j(\mathbf{r})$ is the periodic basis function.[21] The electron-photon interaction is

$$H_{e-p}=\frac{e}{cm_0}\mathbf{A}\cdot\mathbf{P} . \tag{A2}$$

According to Fermi's golden rule, the optical transition rate between the nth subband and n'th subband is

$$R=\frac{2\pi}{\hbar}|\langle\Psi_n|H_{e-p}|\Psi_{n'}\rangle|^2\delta(E_{n'}-E_n-\hbar\omega) . \tag{A3}$$

Substituting Eq. (A1) into Eq. (A3), one can have[15]

$$\begin{aligned}\langle\Psi_n|H_{e-p}|\Psi_{n'}\rangle&=\frac{e\mathbf{A}}{cm_0}\cdot\sum_{j,j'}(\langle F_{nj}|\mathbf{P}|F_{n'j'}\rangle\langle U_j|U_{j'}\rangle\\&\quad+\langle F_n|F_{n'j'}\rangle\langle U_j|\mathbf{P}|U_{j'}\rangle)\\&=\frac{e\mathbf{A}}{cm_0}\cdot\sum_{j,j'}(\langle F_{nj}|\mathbf{P}|F_{n'j'}\rangle\delta_{ij}\\&\quad+\langle F_{nj}|F_{n'j'}\rangle\mathbf{P}_{jj'})\end{aligned} \tag{A4}$$

where $\mathbf{P}_{jj'}$ are matrix elements of the momentum with respect to the periodic basis functions $U_j(\mathbf{r})$. Considering the intersubband transitions in the conduction band, the conduction-band envelope function F_{nc} associated with $U_c(\mathbf{r})$ is dominant among all $F_{nj}(\mathbf{r})$. Neglecting spin-orbit interaction, the small envelope functions $F_{nr}(\mathbf{r})$ are given by[21]

$$\begin{aligned}F_{nr}(\mathbf{r})\approx[E_n-H_{rr}(\mathbf{r})]^{-1}[m_0^{-1}\mathbf{P}_{rc}\cdot\mathbf{P}F_{nc}(\mathbf{r})\\+H_{rc}(\mathbf{r})F_{nc}(\mathbf{r})] ,\end{aligned} \tag{A5}$$

where $H_{jj'}(\mathbf{r})$ are the corresponding matrix elements of the periodic crystal Hamiltonian of the material at $\mathbf{r}$,[21] the subscript r denotes remote bands, i.e., all bands other than the conduction band described in Ref. 21. From symmetry consideration, one can only obtain a nonzero $F_{nr}(\mathbf{r})$ for r corresponding to a basis function of either Γ_1 or Γ_{15} symmetry. For Γ_1 symmetry, one obtains $\mathbf{P}_{rc}=0$ and

$$F_{nr}(\mathbf{r})\approx[E_n-H_{rr}(\mathbf{r})]^{-1}H_{rc}(\mathbf{r})F_{nc}(\mathbf{r}) . \tag{A6}$$

For Γ_{15} symmetry, one obtains

$$F_{nr}(\mathbf{r})\approx[E_n-H_{rr}(\mathbf{r})]^{-1}m_0^{-1}\mathbf{P}_{rc}\cdot\mathbf{P}F_{nc}(\mathbf{r}) . \tag{A7}$$

Thus one can obtain

$$\begin{aligned}\langle\Psi_n|H_{e-p}|\Psi_{n'}\rangle&=\frac{e\mathbf{A}}{cm_0}\cdot\left[\sum_j\langle F_{nj}|\mathbf{P}|F_{n'j}\rangle+\sum_{r(\Gamma_{15})}(\langle F_{nc}|F_{n'r}\rangle\mathbf{P}_{cr}+\langle F_{nr}|F_{n'c}\rangle\mathbf{P}_{rc})\right]\\&\quad+\frac{e\mathbf{A}}{cm_0}\cdot\sum_{r(\Gamma_1),r'(\Gamma_{15})}(\langle F_{nr}|F_{n'r'}\rangle\mathbf{P}_{rr'}+\langle F_{nr'}|F_{n'r}\rangle\mathbf{P}_{r'r}) .\end{aligned} \tag{A8}$$

From Eqs. (A6) and (A7), one can see that the last term corresponding to $\langle F_{nr}|F_{n'r'}\rangle$ in Eq. (A8) is a higher-order small quantity and can be neglected. Using Eq. (A7), one obtains

$$\langle \Psi_n | H_{e-p} | \Psi_{n'} \rangle \approx \frac{e\mathbf{A}}{cm_0} \cdot \sum_j \langle F_{nj} | \mathbf{P} | F_{n'j} \rangle + \frac{e\mathbf{A}}{cm_0} \cdot \sum_{r(\Gamma_{15})} \frac{\mathbf{P}_{rc} \cdot \mathbf{P}_{cr}}{m_0} (\langle F_{nc} | [E_{n'} - H_{rr}]^{-1} \mathbf{P} F_{n'c} \rangle + \langle [E_n - H_{rr}]^{-1} \mathbf{P} F_{nc} | F_{n'c} \rangle) . \quad \text{(A9)}$$

In the multiband model, an energy-dependent effective mass $m_c(E,\mathbf{r})$ is given by[21]

$$\frac{m_0}{m_c(E,\mathbf{r})} = 1 + 2 \sum_{r(\Gamma_{15})} \frac{\mathbf{P}_{rc} \cdot \mathbf{P}_{cr}}{m_0} [E - H_{rr}]^{-1} . \quad \text{(A10)}$$

Substituting Eq. (A10) into Eq. (A9) and noticing that $\mathbf{P}$ is a Hermitian operator, one obtains

$$\langle \Psi_n | H_{e-p} | \Psi_{n'} \rangle \approx \frac{e\mathbf{A}}{cm_0} \cdot \sum_j \langle F_{nj} | \mathbf{P} | F_{n'j} \rangle + \frac{e\mathbf{A}}{cm_0} \cdot \langle F_{nc} | \left[\frac{m_0 - m_c(E_{n'},\mathbf{r})}{2m_c(E_{n'},\mathbf{r})} \mathbf{P} + \mathbf{P} \frac{m_0 - m_c(E_n,\mathbf{r})}{2m_c(E_n,\mathbf{r})} \right] | F_{n'c} \rangle . \quad \text{(A11)}$$

For only the conduction band, we focus on the spatial dependence of the effective mass and neglect its energy dependence. Hence the energy-dependent effective mass $m_c(E,\mathbf{r})$ is replaced by an energy-independent effective mass $m^*(\mathbf{r})$ in the one-band model. For semiconductor materials of interest, the electron effective mass m^* is much less than the free-electron mass m_0, and the second term in Eq. (A11) makes a dominant contribution to the optical intersubband transition. Therefore, under the effective-mass approximation, Eq. (A11) can be rewritten as

$$\langle \Psi_n | H_{e-p} | \Psi_{n'} \rangle \approx \frac{e\mathbf{A}}{2c} \cdot \langle F_{nc} | \left[\frac{1}{m^*(\mathbf{r})} \mathbf{P} + \mathbf{P} \frac{1}{m^*(\mathbf{r})} \right] | F_{n'c} \rangle = \langle F_{nc} | H_{\text{int}} | F_{n'c} \rangle . \quad \text{(A12)}$$

This means that one can introduce the effective electron-photon interaction Hamiltonian H_{int} indicated in Eq. (3), together with only conduction-band envelope functions, for the optical intersubband transitions in the conduction-band QW heterostructures.

[1]For example, see reviews, in *Intersubband Transitions in Quantum Wells,* edited by E. Rosencher, B. Vinter, and B. F. Levine (Plenum, New York, 1992).

[2]Y.-C. Chang and R. B. James, Phys. Rev. B **39**, 12 672 (1989).

[3]B. F. Levine, S. D. Gunapala, J. M. Kuo, S. S. Pei, and S. Hui, Appl. Phys. Lett. **59**, 1864 (1991).

[4]S. D. Gunapala, B. F. Levine, D. Ritter, R. Hamm, and M. B. Panish, J. Appl. Phys. **71**, 2458 (1992).

[5]J. Katz, Y. Zhang, and W. I. Wang, Electron. Lett. **28**, 932 (1992).

[6]C.-L. Yang, D.-S. Pan, and R. Somoana, J. Appl. Phys. **65**, 3253 (1989).

[7]J. S. Park, R. P. G. Karunasiri, and K. L. Wang, Appl. Phys. Lett. **60**, 103 (1992).

[8]L. A. Samoska, B. Brar, and H. Kroemer, Appl. Phys. Lett. **62**, 2539 (1993).

[9]Y. Zhang, N. Baruch, and W. I. Wang, Appl. Phys. Lett. **63**, 1068 (1993).

[10]F. T. Vas'ko and Y. N. Soldateno, Fiz. Tekh. Poluprovodn. **20**, 920 (1986) [Sov. Phys. Semicond. **20**, 579 (1986)], where the possibility of the in-plane polarized optical intersubband transition due to the spatial variation of the effective mass was pointed out. However, this mechanism was much less exploited there, of which little appreciation has been expressed in the literature.

[11]M. Zaluzny, Solid State Commun. **57**, 619 (1986).

[12]A. Shik, Fiz. Tekh. Poluprovodn. **22**, 1843 (1988) [Sov. Phys. Semicond. **22**, 1165 (1988)].

[13]R. P. Leavitt, Phys. Rev. B **44**, 11 270 (1991).

[14]L. H. Peng, J. H. Smet, T. P. E. Broekaert, and C. G. Fonstad, Appl. Phys. Lett. **62**, 2413 (1993).

[15]Rui Q. Yang, J. M. Xu, and M. Sweeny, Phys. Rev. B **50**, 7474 (1994), where the terms arising merely from the spatial variation of band-structure parameters are missing in Eqs. (26) and (34a) which are insignificant similar to M_{za} as shown in this paper.

[16]Rui Q. Yang, Appl. Phys. Lett. **66**, 959 (1995).

[17]L. H. Peng, J. H. Smet, T. P. E. Broekaert, and C. G. Fonstad, Appl. Phys. Lett. **61**, 2078 (1992).

[18]H. S. Li, R. P. G. Karunasiri, Y. W. Chen, and K. L. Wang, J. Vac. Sci. Technol. B **11**, 922 (1993).

[19]Z. Chen, M. Li, D. Cui, H. Lu, and G. Yang, Appl. Phys. Lett. **62**, 1502 (1993).

[20]D. J. BenDaniel and C. B. Duke, Phys. Rev. **152**, 683 (1966).

[21]B. G. Burt, Phys. Rev. B **50**, 7518 (1994).

[22]G. Bastard, *Wave Mechanics Applied to Semiconductor Heterostructures* (Les Editions de Physique, Les Ulis, 1988).

[23]W. Kohn, in *Solid State Physics,* edited by F. Seitz and D. Turnbull (Academic, New York, 1957), Vol. 5, p. 257.

[24]H. C. Liu, J. Appl. Phys. **73**, 3062 (1993); (unpublished).

[25]L. C. West and S. J. Eglash, Appl. Phys. Lett. **46**, 1156 (1985).

[26]S. Datta, *Quantum Phenomena* (Addison-Wesley, New York,

1989).
[27]R. E. Doezema and H. D. Drew, Phys. Rev. Lett. **57**, 762 (1986).
[28]Z. Ikonic, V. Milanovic, D. Tjapkin, and S. Pajevic, Phys. Rev. B **37**, 3097 (1988).
[29]L. D. Landau and E. M. Lifshitz, *Quantum Mechanics* (Pergamon, New York, 1965), Chap. 3.
[30]L. C. Lew Yan Voon, M. Willatzen, and L. R. Ram-Mohan, J. Appl. Phys. **78**, 295 (1995).
[31]V. Berger, P. Bois, and E. Rosencher, Appl. Phys. Lett. **64**, 800 (1994).

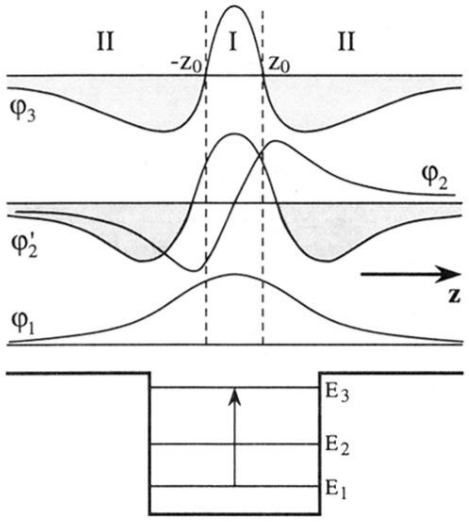

FIG. 3. Schematic illustration of eigenfunctions φ_1, φ_3, φ_2 and its derivative φ_2' (upper part), and the square QW (lower part).